IEEE Photonics Journal
An IEEE Photonics Society Publication

Open Access

A Modified Empirical Mode Decomposition Algorithm in TDLAS for Gas Detection

Volume 6, Number 6, December 2014

Yunxia Meng
Tiegen Liu
Kun Liu
Junfeng Jiang
Ranran Wang
Tao Wang
Haofeng Hu

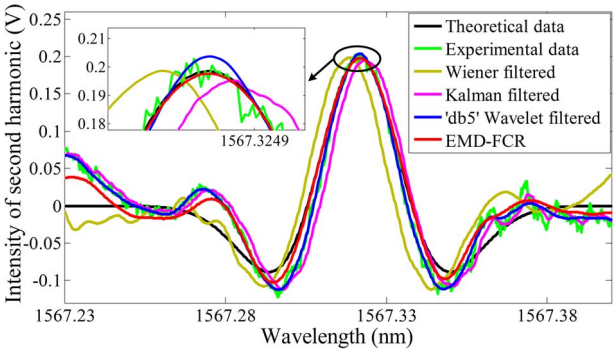

DOI: 10.1109/JPHOT.2014.2368785
1943-0655

A Modified Empirical Mode Decomposition Algorithm in TDLAS for Gas Detection

Yunxia Meng,[1,2] Tiegen Liu,[1,2] Kun Liu,[1,2] Junfeng Jiang,[1,2] Ranran Wang,[1,2] Tao Wang,[1,2] and Haofeng Hu[1,2]

[1]College of Precision Instrument and Opto-Electronics Engineering, Tianjin University, Tianjin 300072, China
[2]Key Laboratory of Opto-electronics Information Technology of Ministry of Education, Tianjin University, Tianjin 300072, China

DOI: 10.1109/JPHOT.2014.2368785

Manuscript received September 2, 2014; revised October 22, 2014; accepted November 1, 2014. Date of publication November 10, 2014; date of current version November 21, 2014. This work was supported in part by the National Basic Research Program of China under Grant 2010CB327802; by the National Natural Science Foundation of China under Grant 61108070, Grant 61227011, Grant 61378043, and Grant 61475114; by the National Instrumentation Program under Grant 2013YQ030915; by the Tianjin Natural Science Foundation under Grant 13JCYBJC16200; by the Science and Technology Key Project of Chinese Ministry of Education under Grant 313038; and by the Shenzhen Science and Technology Research Project under Grant JCYJ20120831153904083. Corresponding author: K. Liu (e-mail: beiyangkl@tju.edu.cn).

Abstract: Based on the research of the traditional empirical mode decomposition (EMD) method, we proposed a modified EMD algorithm for the detected signal processing in tunable diode laser absorption spectroscopy. The modified EMD algorithm introduced Savitzky–Golay filtering and cross-correlation operation into the traditional EMD algorithm and reconstructed the signal by using the cross-correlation coefficients effectively. Based on the modified EMD algorithm in theory, the second harmonic component analysis was simulated by comparing with some other filtering algorithms. The experiments system was performed for carbon monoxide (CO) concentration detection. Comparing the sensing performances without and with using EMD-FCR and other filtered methods, the experimental results show that the signal-to-noise ratio of the system was significantly improved from 7.32 to 14.31 dB by EMD-FCR corresponding to one absorption line of CO at 1567.32 nm, leading to the minimum detection limit of 2 ppm. The accuracy and stability of the system are both improved by proposing the modified EMD algorithm.

Index Terms: Gas, harmonic analysis, filters, correlation, signal reconstruction.

1. Introduction

Gas concentration detection based on Tunable Diode Laser Absorption Spectroscopy (TDLAS) with its good performances of high sensitivity, fast response and high stability, has been widely applied in industrial production, safety and environmental monitoring [1]–[3]. Combined with the wavelength modulation spectroscopy (WMS) technique and harmonic detection technique (HDT), TDLAS can obtain the harmonic components of the absorption line of the detected gases in the near-infrared region. However, the amplitudes of harmonic components are small because gas absorption is weaker in near-infrared than in mid-infrared region [4]. Moreover, a lot of noises from the optical components (etalon fringes) and electronic devices (white Gaussian noises) are imported into harmonic components, which will reduce the signal-to-noise-ratio (SNR) of harmonic components [5], [6]. When the gas concentration is low, the harmonic signal

of demodulation has been drowned into the noises [7]. Therefore, many de-noising methods have been proposed successively. The signal averaging is an early and simply method for signal processing in TDLAS [8], which enhances the stability and improves the detection accuracy limitedly. The Wiener filter employs a minimum mean square error algorithm (MMSE) to optimize a set of the coefficients for the filter, which is able to adapt to the changing conditions such as signal drift and changing background structures [9]. Kalman filter with its adaptability is demonstrated to adapt to the noises and data statistics by adjusting to the changes in signal statistics and dynamic range during operation [10]. Wiener filter and Kalman filter have been proved as powerful tools for signal processing, but taking up large computation cost and storage space. With the application of Wavelet Transform filter in signal processing, better measurement precision and higher detection sensitivity were achieved [11], [12]. However, the selection of wavelet basis and the determination of scales in multiscale analysis have great effects on the quality of the de-noised signal with subjectivity. The above filter methods are designed for linear but non-stationary data or non-linear but stationary and deterministic systems [13]. In the TDLAS system, the gas absorption is a non-linear and non-stationary process with random and non-random noises. On the other hand, the empirical mode decomposition (EMD) method was proposed firstly by Huang *et al*. in 1998 [13], and then had been successfully applied to aerospace, biomedical and other natural sciences with its excellent performance in processing non-stationary and non-linear signal [14]–[16]. Based on the underlying properties of decomposing local oscillations signal into a collection of intrinsic mode functions (IMFs) in time domain, the EMD made up for the inadequacies of other de-noising algorithms. In recent years, the EMD has also been introduced for the gas concentration detection as an efficient tool to remove noises from severely polluted signal [17], [18]. Furthermore, the Savitzky-Golay filter using the least squares fitting coefficient as filter response function, is a totally adaptive filtering method for high frequency noises with convolution smoothing [19].

Thus, combining with the EMD method, Savitzky-Golay filter, cross-correlation and signal reconstruction (FCR), this paper describes the effective approach of applying EMD-FCR algorithm filtering to real-time gas concentration measurements with TDLAS system. Firstly, we presented the formulation and detection procedures of the EMD-FCR algorithm in theory. And then, taking carbon monoxide (CO) gas as an example, we compared the performance differences between the EMD-FCR algorithm filtering and the other general filtering algorithms such as Wiener, Kalman, and Wavelet, by using a pure second harmonic signal with the white Gaussian noises and etalon fringes. The result of the EMD-FCR algorithm is the highest SNR and the closest to the pure second harmonic signal. Finally, we evaluated the performances of the EMD-FCR algorithm experimentally. Comparisons of the sensing performances of without and with using EMD-FCR as well as other filtering algorithms indicate that the EMD-FCR algorithm is an effective processing tool, both for the spectral signal processing and the gas concentration detection.

2. Principles of EMD-FCR Algorithm

The traditional EMD algorithm is a self-adaptive time domain decomposition method without any priori subjective criterion selection [13]. By using the traditional EMD, any complicated signal can be decomposed into a collection of IMFs based on the local characteristic time scale of the signal. The harmonic components of the gas absorption line are the local oscillations signals, which can be decomposed into several IMFs. Each IMF must meet two conditions: 1) In the whole data set, the number of extrema and the number of zero crossings must either equal or differ at most by one; 2) at any point, the mean value of the envelope defined by the local maxima and the envelope defined by the local minima is zero.

In the TDLAS system, the second harmonic signal is used for gas concentration detection, attributing its symmetry about center frequency of absorption line and it is the maximum one in the even-order harmonic components, with more than two orders of magnitude larger than other harmonic components under the optimal modulation depth [4]. Besides, the detected second harmonic signal which contains a lot of noises is a non-stationary and non-linear signal. The

combination of the traditional EMD algorithm and the Savitzky-Golay filter is necessary for the second harmonic signal processing. In order to obtain the filtered signal by using the modified EMD, we need to reconstruct the signal using each filtered IMF and their cross-correlation coefficients. The processing of second harmonic signal through the EMD-FCR algorithm can be divided into four main parts: Firstly, the demodulated second harmonic signal A_2 is decomposed into all possible IMFs components H_i. Secondly, the IMFs H_i are filtered by the Savitzky-Golay method to obtain the filtered signals fH_i. Thirdly, the cross-correlation coefficients C_i between second harmonic signal A_2 and filtered signals fH_i are obtained by cross-correlation operation respectively. And finally, the second harmonic signal is reconstructed by summing the products of fH_i and its corresponding cross-correlation coefficients C_i. The detailed steps are presented as follows:

Step 1. Find out all the local maxima and minima of the second harmonic signal A_2 to obtain the upper envelope $X_{\max}$ and the lower envelope $X_{\min}$, respectively, using the cubic spline interpolation.

Step 2. Compute the mean of the upper and lower envelope $m_1 = (X_{max} + X_{min})/2$, and obtain the difference h_1 between the original signal A_2 and m_1.

Step 3. If h_1 meets the conditions of IMFs, h_1 is the first IMF, which is marked as H_1.

Else, if h_1 does not meet the conditions of IMFs, replace A_2 with h_1. Repeat the steps 1–2 k times until h_{1k} meets the conditions. The h_{1k} is an IMF component, which is marked as H_1.

Step 4. Subtracting the IMF H_1 from the original signal A_2, we obtain the residual signal r_1. Taking r_1 as the original signal, repeat the steps 1–3 until the final component does not meet the conditions of IMFs, which means that the residual signal cannot be further decomposed. The nth IMF can be obtained, where n refers the number of IMFs. The final residual component is the residue of this decomposition, which is marked as r.

By taking the steps above, the original signal A_2 can be decomposed into n IMFs and a residue as follows:

$$A_2 = \sum_{i=1}^{n} H_i + r \tag{1}$$

where the H_i means the ith IMF component, and the n is a finite integer number.

Step 5. Filter each IMF H_i and r by using the Savitzky-Golay method to obtain the filtered signal fH_i and fr.

Step 6. Calculate the cross-correlation coefficients C_i, C_r between the original signal A_2 and each filtered signal fH_i, fr, respectively, through cross-correlation operation.

Step 7. Reconstruct the second harmonic signal R_2 by summing the products of fH_i, fr and its corresponding cross-correlation coefficient C_i (C_r) which was obtained in step 6. That is

$$R_2 = \sum_{i=1}^{n} C_i \cdot fH_i + C_r \cdot fr. \tag{2}$$

The above steps constitute the EMD-FCR algorithm. After the processing of the steps 1–7, we can obtain the filtered second harmonic signal R_2 used for gas concentration detection, in which the noises are sharply suppressing.

3. Simulations and Analysis

Based on the theoretical analysis mentioned above, we took the absorption line of CO at 1567.32 nm, for example. And we simulated the pure second harmonic signal of CO gas and the contaminated signal by comingling the pure second harmonic signal with the white Gaussian

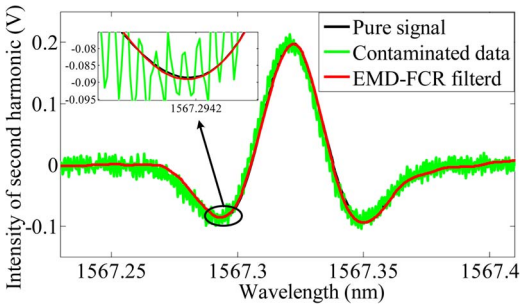

Fig. 1. Simulation second harmonic signals of CO at 1567.32 nm. The black line represents the pure second harmonic signal, the green line represents the contaminated second harmonic signal, and the red line represents the filtered second harmonic signal by EMD-FCR filtered.

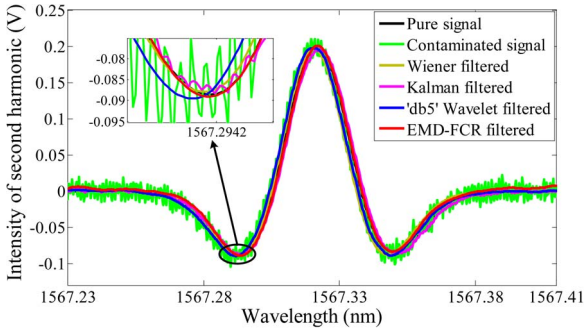

Fig. 2. Filtered second harmonic signals by using different methods. The black line represents the theoretical second harmonic signal, the green line represents the contaminated second harmonic signal, the light green line represents the filtered second harmonic signal by Wiener filtered, the magenta line represents the filtered second harmonic signal by Kalman filtered, the blue line represents the filtered second harmonic signal by "db5" Wavelet filtered, and the red line represents the filtered second harmonic signal by EMD-FCR filtered.

noises under SNR of 22 dB and the etalon fringes of 0.01 V which is closest to the noises signal of the actual system. The relevant parameters at 296 K of the CO absorption line were obtained from HITRAN2008 spectroscopic database [20]. The absorption line intensity of CO at 1567.32 nm is 2.14×10^{-23} $\text{cm}^{-1}/(\text{molecule} \cdot \text{cm}^{-2})$, and the air-broadened half-width is 0.0589 $\text{cm}^{-1}/\text{atm}$. In the standard temperature and pressure, the gas absorption line can be described as the Gaussian line type [3]. We choose the white Gaussian noises because it is typical noises in theory and in the experiments. Fig. 1 shows the simulation results, where 40 ppm CO gas concentration and 20 m effective optical path length are set as simulation parameters.

The black line in Fig. 1 is the theoretical data of pure second harmonic signal of CO gas. To assess the efficiency of the EMD-FCR algorithm, the white Gaussian noises and the etalon fringes are added to the pure second harmonic signal. The green line of Fig. 1 represents the contaminated second harmonic signal, which is A_2 of part 2. After the processing of the steps 1–7 with contaminated signal, we obtained the filtered second harmonic signal, which is shown as the red line of Fig. 1. It can be seen that the filtered second harmonic signal matches the theoretical data perfectly.

The performances of the modified EMD, EMD-FCR, were also tested and compared to the other filtered algorithms. The results are shown in Fig. 2. The contaminated signal (length of 800 points) was processed by using the Wiener filter (transfer function length of seven points, and mean square error threshold of 0.05 V), Kalman filter (transfer coefficient of 1.02 in the initial state, system disturbance coefficient of 3 in the initial state, observational coefficient of 1.15 in

TABLE 1
SNR and residual sum of squares (SSR) of different filters

Filter	Wiener	Kalman	Wavelet	EMD-FCR
SNR_1(dB)	14.17	11.21	13.26	14.82
$SSR_1(V^2)$	0.0287	0.3010	0.0027	0.0014
SNR_2(dB)	14.02	11.81	13.96	14.31
$SSR_2(V^2)$	0.9859	0.7523	0.5943	0.2538

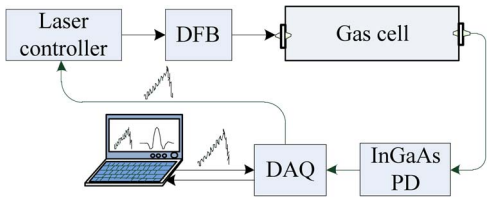

Fig. 3. The configuration of TDLAS with SLIDA for gas detection.

the initial state, q-value of 100), and "db5" Wavelet filter ("db5" wavelet basis with heursure of soft-threshold, decomposition level of 5). The SNR_1 and residual sums of squares SSR_1 corresponding to the pure and the filtered signals are obtained in Table 1. It is found that of all filtered curves, the one filtered by our method is the highest SNR and the closest to the real theoretical line. However, it should be pointed out that the above comparisons are only based on the Gaussian line type.

4. Experiment and Discussion

In order to evaluate the performances of the EMD-FCR algorithm experimentally, a series of experiments were carried out based on the TDLAS system with Software Lock-In Demodulation Algorithm (SLIDA). The configuration of TDLAS using the SLIDA for CO gas concentration detection is shown in Fig. 3. The output of the DAQ card (NI-6361) generated a driving voltage signal composited by a 1 Hz low-frequency sawtooth wave and a 2 KHz high-frequency cosine wave. The laser controller (LSI-XX50, ETSC) was driven by the DAQ card with 16-bit DAC resolution and transferred the voltage signal into the current signal with the transfer coefficient of 50 mA/V. The DFB laser (NLK1L5GAAA, NEL) with a power of 20 mW emitted single mode radiation at 1567.32 nm by the laser controller. The laser controller was modulated by current signal under the tuning coefficient of 5.2 pm/mA. The gas cell (163-20XX, PIKE) with the effective optical length of 20 m, was filled with CO of 40 ppm concentration in standard atmospheric pressure. The Photo-detector (PDA10CS-EC, Thorlabs) received the transmitted light and transformed it into an electrical signal for further processing. The input of the DAQ card with 16-bit resolution collected the signal from the PD output, and sent the data into the PC based on the USB bus. The output and input of the DAQ card were working synchronously with the same clock. The modulation amplitude of the cosine wave was set as 19 mA, which was in accordance with the optimized modulation depth, and the operating temperature of laser was set to a constant value of 22 °C. In order to make the wavelength tuning range of laser is from 1567.20 nm to 1567.45 nm, the corresponding current tuning range was set from 70 mA to 118 mA (the tuning range of sawtooth wave). The second harmonic component is obtained in 0.1 s by LabVIEW software based on the SLIDA with the modulation frequency of 2 KHz.

By using the SLIDA mentioned above, the second harmonic signal A_2 of 40 ppm CO gas at 1567.32 nm was obtained, as shown in Fig. 4(a). It can be seen that the original second

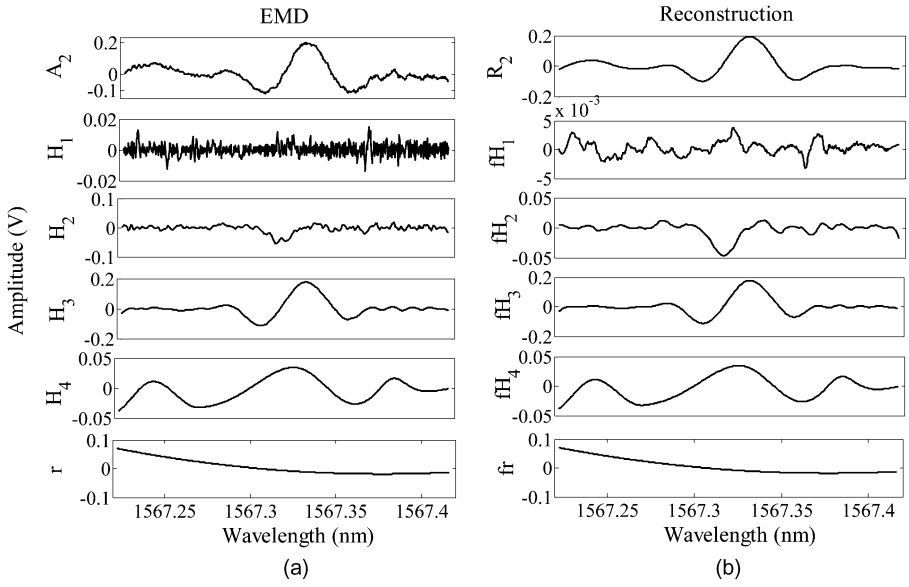

Fig. 4. (a) Original data and its intrinsic mode functions (IMFs) by EMD. (b) Reconstruction signal by EMD-FCR algorithm and filtered IMFs by Savitzky-Golay method.

TABLE 2

Cross-correlation coefficients

IMFs	H_1	H_2	H_3	H_4	r
$C_i(C_r)$	0.20	0.17	0.92	0.44	0.41

harmonic signal has a lower SNR, leading to a deteriorative minimum detection limit (MDL) of the gas. Therefore, we need to process the original second harmonic signal to improve the SNR and to decrease the MDL of gas detection.

By using the steps 1–4 of theoretical analysis, we obtained the IMFs of the original signal A_2. The filtered IMFs and the reconstruction of the filtered second harmonic signal R_2 were obtained through the steps 5–7, which were mentioned in part 2. The results are shown in Fig. 4.

Fig. 4(a) is the process of decomposition by using EMD. The terminated condition of decomposition is that the residual signal does not meet the conditions of IMFs. According to the above requirements, the original second harmonic signal of 40 ppm CO gas was decomposed into four IMFs and a residue. The H_1, H_2 are the high-frequency parts of second harmonic signal, and the H_3, H_4, r are the low frequency parts. The Fig. 4(b) shows the filtered IMFs by the Savitzky-Golay method.

Table 2 lists the cross-correlation coefficients C_i, C_r. It can be seen that the cross-correlation coefficients C_1 and C_2 are less than 0.2, which means H_1 and H_2 contain the high frequency noises. The C_3, C_4, and C_r are greater than 0.4, which means H_3, H_4 and r include the information of the gas concentration. According to Table 2 and Fig. 4(b), we obtained the reconstruction signal R_2 of the second harmonic signal by (2). The filtered signals were also obtained by using other filtered algorithms with the simulation parameters. The SNR_2 and SSR_2 corresponding to filtered and theoretical signals were listed in Table 1. It can be seen that the result of EMD-FCR filtered is the highest SNR and the closest to the theoretical line. The results are shown in Fig. 5. It can be seen that the second harmonic signal of CO gas was not symmetric about its own peak value. The left valley was not equal to the right one due to the influences of the residual amplitude modulation and the intensity modulation [21]. The SNR_2 of reconstruction signal R_2 is 14.31 dB. It can be seen that the EMD-FCR algorithm not only restrained the noises to

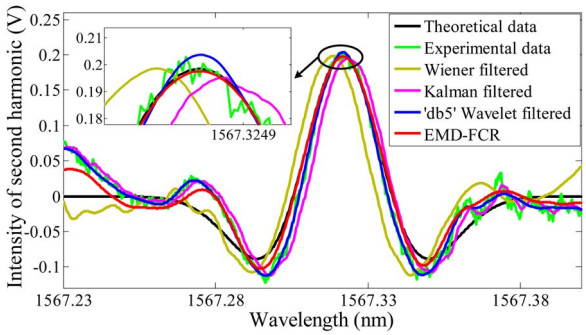

Fig. 5. Experimental data of second harmonic signal and its filtered signals. The black line is the theoretical second harmonic signal, the green line represents the experimental data, the light green line represents the filtered second harmonic signal by Wiener filtered, the magenta line represents the filtered second harmonic signal by Kalman filtered, the blue line represents the filtered second harmonic signal by "db5" Wavelet filtered, and the red line represents the filtered second harmonic signal by EMD-FCR filtered.

TABLE 3

Comparisons of system performance parameters

Parameters	SNR(dB)	MDL(ppm)	R^2
Original data	7.32	18	0.93290
EMD-FCR	14.31	2	0.99297

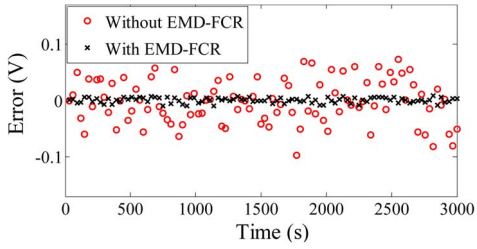

Fig. 6. Demodulation error of second harmonic intensity of without and with using EMD-FCR algorithm in 50 minutes.

increase the SNR of second harmonic signal but also drew the baseline to zero to obtain the reconstruction signal efficiently. The SNR of second harmonic component was improved from 7.32 dB to 14.31 dB with the enhancement of 7 dB, which is shown in Table 3.

Fig. 6 shows the errors of second harmonic intensity in 50 minutes without and with using EMD-FCR algorithm. The mean square errors are 0.0015 V and 2.113×10^{-5} V respectively. It can be seen that the errors of the second harmonic intensity using EMD-FCR algorithm was reduced greatly compared with that of the one without using the EMD-FCR algorithm. It means that, the accuracy and the stability of the system were both improved significantly.

To further verify the performances of the EMD-FCR algorithm, we performed the CO gas detection experiments under different concentrations. As the CO gas concentration in the gas cell changed from 20 ppm to 200 ppm with the interval of 20 ppm, the amplitudes of the second harmonic signal were obtained as shown in Fig. 7. It can be seen that the relationship between the amplitude of the second harmonic signal and gas concentration is linear with the slope of 0.00542 V/ppm. The linear correlation coefficient R^2 was improved from 0.93290 of the original data to 0.99297 of the filtered one by using EMD-FCR algorithm. The results of the linear correlation coefficients are shown in Table 3.

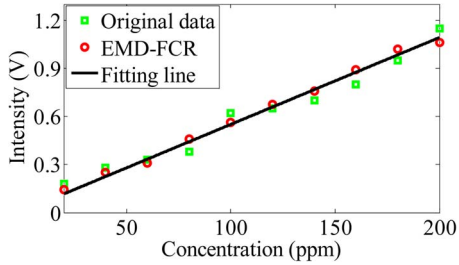

Fig. 7. Relationship between the second harmonic intensity and gas concentration.

According to the linear relationship between the amplitude of the second harmonic signal and gas concentration, we defined the formula to calculate the MDL of the system as follows:

$$MDL = \frac{1}{K} \cdot 2A_{noise} \tag{3}$$

where A_{noise} is the amplitude of the noises, and K is the slope of the fitting line. From (3), the MDLs of the original second harmonic signal and reconstruction signal were obtained with 18 ppm and 2 ppm respectively.

This EMD-FCR algorithm is an efficient tool to remove noises from the original signal. It greatly improved the SNR of the second harmonic signal and decreased the MDL of the system. Furthermore the EMD-FCR algorithm can also be used for other non-stationary and non-linear signal processing.

5. Conclusion

In this paper, we introduced the EMD-FCR algorithm into the TDLAS system for gas detection. Based on the traditional EMD method and combined with filter correlation as well as reconstruction algorithm the EMD-FCR algorithm was presented in theory. Taking CO gas at 1567.32 nm as example we simulated the contaminated second harmonic signal by comingling the pure second harmonic signal and the white Gaussian noises as well as etalon fringes. With the filtering methods applied to the simulation signal such as Wiener Kalman Wavelet and EMD-FCR algorithm filtering we draw a conclusion that the EMD-FCR algorithm could obtain the highest SNR and the closest curve to the pure second harmonic signal. In order to evaluate the performances of the EMD-FCR algorithm experimentally a series of experiments were carried out based on the TDLAS system. Compared the sensing performances under the case without and with using EMD-FCR as well as other filtered methods the results indicated that the SNR was significantly improved from 7.32 dB to 14.31 dB by EMD-FCR and the MDL decreased from 18 ppm to 2 ppm with SNR = 3 dB. By using the EMD-FCR algorithm the relationship between the amplitude of second harmonic signal and the gas concentration is linear with the linear correlation coefficient of 0.99297. The results showed that this EMD-FCR algorithm kept its original spectral features and had a better SNR and MDL.

References

[1] B. Culshaw, G. Stewart, F. Dong, C. Tandy, and D. Moodie, "Fibre optic techniques for remote spectroscopic methane detection—From concept to system realisation," *Sens. Actuators B, Chem.*, vol. 51, no. 1–3, pp. 25–27, Aug. 1998.
[2] K. B. Dinh, P. Hannaford, and L. Van Dao, "Phase-matched high harmonic generation for the study of rotational coherence molecular dynamics," *Opt. Commun.*, vol. 284, no. 14, pp. 3607–3611, Jul. 2011.
[3] L. Li, N. Arsad, G. Stewart, G. Thursby, B. Culshaw, and Y. Wang, "Absorption line profile recovery based on residual amplitude modulation and first harmonic integration methods in photoacoustic gas sensing," *Opt. Commun.*, vol. 284, no. 1, pp. 312–316, Jan. 2011.
[4] J. Reid and D. Labrie, "Second-harmonic detection with tunable diode lasers—Comparison of experiment and theory," *Appl. Phys. B*, vol. 26, no. 3, pp. 203–210, Nov. 1981.

[5] D. Masiyano, J. Hodgkinson, S. Schilt, and R. P. Tatam, "Self-mixing interference effects in tunable diode laser absorption spectroscopy," *Appl. Phys. B*, vol. 96, no. 4, pp. 863–874, Aug. 2009.
[6] H. Riris, C. B. Carlisle, R. E. Warren, and D. E. Cooper, "Signal-to-noise ratio enhancement in frequency-modulation spectrometers by digital signal processing," *Opt. Lett.*, vol. 19, no. 2, pp. 144–146, Jan. 1994.
[7] X. T. Lou *et al.*, "Simultaneous detection of multiple-gas species by correlation spectroscopy using a multimode diode laser," *Opt. Lett.*, vol. 35, no. 11, pp. 1749–1751, Jun. 2010.
[8] P. Werle, R. Mücke, and F. Slemr, "The limits of signal averaging in atmospheric trace-gas monitoring by tunable diode-laser absorption spectroscopy (TDLAS)," *Appl. Phys. B*, vol. 57, no. 2, pp. 131–139, Aug. 1993.
[9] P. W. Werle, B. Scheumann, and J. Schandl, "Real-time signal-processing concepts for trace-gas analysis by diode-laser spectroscopy," *Opt. Eng.*, vol. 33, no. 9, pp. 3093–3105, Sep. 1994.
[10] D. P. Leleux, R. Claps, W. Chen, F. K. Tittel, and T. L. Harman, "Applications of Kalman filtering to real-time trace gas concentration measurements," *Appl. Phys. B*, vol. 74, no. 1, pp. 85–93, Jan. 2002.
[11] J. Li, U. Parchatka, and H. Fischer, "Applications of wavelet transform to quantum cascade laser spectrometer for atmospheric trace gas measurements," *Appl. Phys. B*, vol. 108, no. 4, pp. 951–963, Sep. 2012.
[12] G. Tian and J. Li, "Tunable diode laser spectrometry signal de-noising using discrete wavelet transform for molecular spectroscopy study," *Opt. Appl.*, vol. 43, no. 4, pp. 803–815, Oct. 2013.
[13] N. E. Huang *et al.*, "The empirical mode decomposition and the Hilbert spectrum for nonlinear and non-stationary time series analysis," *Proc. R. Soc. Lond. A, Math. Phys. Sci.*, vol. 454, no. 1971, pp. 903–995, Mar. 1998.
[14] D. Pines and L. Salvino, "Structural health monitoring using empirical mode decomposition and the Hilbert phase," *J. Sound Vib.*, vol. 294, no. 1/2, pp. 97–124, Jun. 2006.
[15] S. Poungponsri and X. H. Yu, "An adaptive filtering approach for electrocardiogram (ECG) signal noise reduction using neural networks," *Neurocomputing*, vol. 117, pp. 206–213, Oct. 2013.
[16] S. Lingfang and W. Yechi, "Soft-sensing of oxygen content of flue gas based on mixed model," *Energy Procedia*, vol. 17, pp. 221–226, 2012.
[17] Q. Xie, J. Li, X. Gao, and J. Jia, "Real time infrared gas detection based on a modified EMD algorithm," *Sens. Actuators B, Chem.*, vol. 136, no. 2, pp. 303–309, Mar. 2009.
[18] C. T. Zheng *et al.*, "Performance improvement of a near-infrared CH_4 detection device using wavelet-denoising-assisted wavelength modulation technique," *Sens. Actuators B, Chem.*, vol. 190, pp. 249–258, Jan. 2014.
[19] A. Savitzky and M. J. E. Golay, "Smoothing and differentiation of data by simplified least squares procedures," *Anal. Chem.*, vol. 36, no. 8, pp. 1627–1639, Jul. 1964.
[20] L. S. Rothman and I. E. Gordon, "The HITRAN 2008 molecular spectroscopic database," *J. Quant. Spectrosc. Radiat. Transf.*, vol. 110, no. 9/00, pp. 533–572, Jun. 2009.
[21] G. Stewart, W. Johnstone, J. R. Bain, K. Ruxton, and K. Duffin, "Recovery of absolute gas absorption line shapes using tunable diode laser spectroscopy with wavelength modulation—Part I: Theoretical analysis," *J. Lightw. Technol.*, vol. 29, no.6, pp. 811–821, Apr. 2011.